



## OPEN ACCESS

EDITED BY  
Houkun Liang,  
Sichuan University, China

REVIEWED BY  
Yijie Shen,  
University of Southampton,  
United Kingdom  
Chaoliang Ding,  
Luoyang Normal University, China

\*CORRESPONDENCE  
Deyuan Shen,  
✉ mrde@jsnu.edu.cn

SPECIALTY SECTION  
This article was submitted  
to Optics and Photonics,  
a section of the journal  
Frontiers in Physics

RECEIVED 08 December 2022  
ACCEPTED 13 January 2023  
PUBLISHED 02 February 2023

CITATION  
Ding M, Wang J, Wang F, Shen D, Tang D  
and Zhu H (2023), High-power Er:Y<sub>2</sub>O<sub>3</sub>  
ceramic laser with an optical vortex beam  
output at ~ 2.7 μm.  
*Front. Phys.* 11:1119263.  
doi: 10.3389/fphy.2023.1119263

COPYRIGHT  
© 2023 Ding, Wang, Wang, Shen, Tang and  
Zhu. This is an open-access article  
distributed under the terms of the [Creative  
Commons Attribution License \(CC BY\)](https://creativecommons.org/licenses/by/4.0/).  
The use, distribution or reproduction in  
other forums is permitted, provided the  
original author(s) and the copyright  
owner(s) are credited and that the original  
publication in this journal is cited, in  
accordance with accepted academic  
practice. No use, distribution or  
reproduction is permitted which does not  
comply with these terms.

# High-power Er:Y<sub>2</sub>O<sub>3</sub> ceramic laser with an optical vortex beam output at ~ 2.7 μm

Manman Ding<sup>1,2</sup>, Jun Wang<sup>3</sup>, Fei Wang<sup>2,4</sup>, Deyuan Shen<sup>2,3\*</sup>,  
Dingyuan Tang<sup>3</sup> and Heyuan Zhu<sup>1</sup>

<sup>1</sup>Department of Optical Science and Engineering, Fudan University, Shanghai, China, <sup>2</sup>Jiangsu Collaborative Innovation Center of Advanced Laser Technology and Emerging Industry, Xuzhou, China, <sup>3</sup>Jiangsu Key Laboratory of Advanced Laser Materials and Devices, School of Physics and Electronic Engineering, Jiangsu Normal University, Xuzhou, China, <sup>4</sup>Jiangsu Institute of Mid Infrared Laser Technology and Applications, Xuzhou, China

We report on the direct generation of the high-power optical vortices at ~2.7 μm from an Er:Y<sub>2</sub>O<sub>3</sub> ceramic laser end-pumped by an annular pump beam using a simple capillary fiber-based pump beam conditioning scheme. Taking advantage of the thermal gradient on the gain medium and mode matching between the pump and oscillating modes, vortex beams with a controllable topological charge order of  $l = 1$  and  $l = 2$  were successfully achieved. The laser yields 4.65 W of output power at an absorbed power of 19.8 W, corresponding to a slope efficiency of 25.9% with respect to the absorbed pump power. Adaptable beam profiles from a shallow crater-shape to quasi-top-hat intensity patterns were directly produced by actively defining the gain distribution in the ceramic, generating 4-W shallow crater-shape beams and 3.9-W quasi-top-hat beams, corresponding to a slope efficiency of 22.0% and 22.7%, respectively. Such optical vortices and tailored spatial intensity profiles in the 3-μm spectral region will enable novel applications, such as super-resolution molecular spectroscopy and material processing.

## KEYWORDS

optical vortices, 2.7 μm, high-power laser, Er:Y<sub>2</sub>O<sub>3</sub> ceramic, annular pumping

## 1 Introduction

Optical vortices characterized by a helical phase variation and a donut intensity spatial distribution carry orbital angular momentum (OAM) of  $l\hbar$  per photon in the beam, where  $l$  is the topological charge or vortex order [1–3]. Coherent sources of the vortex at different wavelengths have found widespread applications in science and technology, including the presence of an extra degree of freedom for improving the channel capacity in optical communications [4], quantum communications [5], super-resolution optical microscopy [6], optical trapping, and manipulation [7, 8]. In particular, optical vortex sources that operate in the mid-infrared region, where rich spectroscopic signatures exist [9, 10], will open up the prospects for super-resolution molecular spectroscopy and microstructure fabrication. Common methods used for generating optical vortices are mainly based on external mode converters, such as spiral phase plates (SPPs) [11], q-plates [12], cylindrical lenses [13], or spatial light modulators (SLMs) [4]. These techniques suffer from at least one of the common drawbacks, such as low wavelength coverage, power handling limitation, and high cost. For example, material dispersion restricts SPP's effectiveness to discrete wavelengths, and thus, it is difficult to produce broadband vortices. SLMs and q-plates usually suffer from a low damage threshold and thus are difficult for high-power operation. Non-linear frequency conversion techniques [14–16], i.e., optical parametric oscillators (OPO) or optical

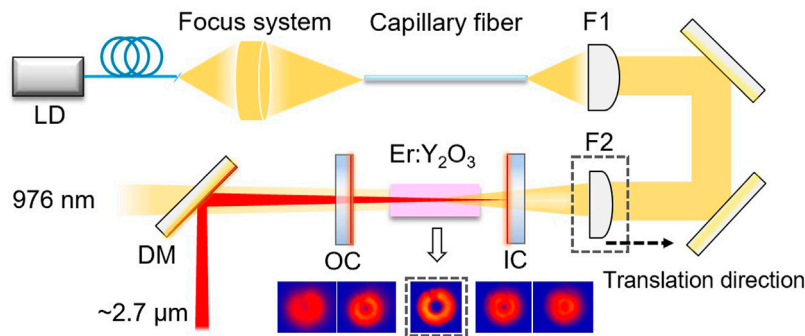


**FIGURE 1**  
Schematic diagram of the Er:Y<sub>2</sub>O<sub>3</sub> ceramic laser.

parametric amplifiers (OPAs), could be an alternative way, providing high power and wavelength-versatile vortices, while the generated topological charge depends highly on the input near-infrared vortex beams [16].

In recent years, “direct generation” techniques have evolved as a simple and efficient route for producing optical vortices [17–20]. Employing a spatially structured pump beam based on a mode-matching principle, optical vortices can be directly generated in a robust laser resonator with advantages of power scalability and high beam quality [18–20]. So far, great efforts have been made to produce optical vortices in the visible and near-infrared spectral regions [18–22], while the exploitation of vortex beams in the mid-infrared spectral region is relatively scarce. In 2019, the first 2.7- $\mu\text{m}$  optical vortex beam was directly generated from an Er:Y<sub>2</sub>O<sub>3</sub> ceramic laser and due to the additional insertion loss and serious thermal issues, the output power of the LG<sub>01</sub> mode was less than 125 mW [23]. Recently, by using polycrystalline Fe:ZnSe as a saturable absorber (SA), the Q-switched LG<sub>01</sub> mode from a 2.7- $\mu\text{m}$  Er:YAP laser was demonstrated [24].

In this paper, we demonstrate the high-power optical vortex operation of an Er:Y<sub>2</sub>O<sub>3</sub> ceramic laser at  $\sim 2.7 \mu\text{m}$ . A ring-shaped pump beam was employed to spatially match the desired LG<sub>01</sub> mode in the laser resonator. Benefits from mode matching between the pump and lasing mode and proper thermal gradient on the ceramic, controllable topological charge order of  $l = 1$  and  $l = 2$  are successfully produced. The laser generated 4.65 W of output power for an absorbed power of 19.8 W, corresponding to a slope efficiency of 25.9% with respect to the absorbed pump power. Direct generation of adaptable beam profiles from a shallow crater shape to quasi-top-hat intensity patterns are achieved by actively defining the gain distribution in the ceramic. The laser produced 4 W of output with shallow crater-shape intensity profiles and 3.9 W of quasi-top-hat intensity profiles, corresponding to a slope efficiency of 22.0% and 22.7%, respectively. This study, to the best of our knowledge, represents the highest output power of optical vortices directly generated from a solid-state oscillator in the 3- $\mu\text{m}$  region and the first direct generation of adaptable beam profiles in this spectral region.

## 2 Experimental setup

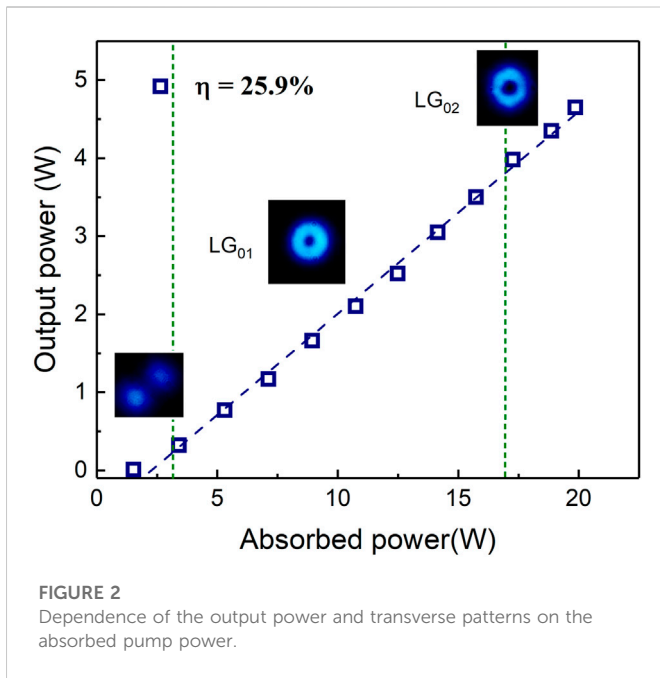
Schematic representation of the experimental setup is shown in Figure 1. An Er:Y<sub>2</sub>O<sub>3</sub> ceramic which was grown in the house *via* co-precipitation with an Er<sup>3+</sup> doping level of 7.0 at% and length 13.5 mm

was used as the gain medium. Furthermore, details can be found in [25]. The ceramic was water-cooled using a copper heat sink maintained at a temperature of 15°C to alleviate thermal loading. The pump source was provided by a high-brightness 976-nm laser diode with a delivery fiber of 105- $\mu\text{m}$  core and 0.22 NA. The output of the laser diode was spectrally narrowed, and the wavelength was stabilized with a volume Bragg grating to have a line width of  $\sim 0.3$  nm. To produce the required ring-shaped beam profile, the output from the laser diode was launched into the annular waveguide of a capillary fiber with a 300- $\mu\text{m}$  diameter inner-cladding and a 110- $\mu\text{m}$ -diameter air-hole in the center. The reformatted pump beam from the capillary fiber was imaged into the Er:Y<sub>2</sub>O<sub>3</sub> ceramic using a telescope configuration with a waist outer radius of  $\sim 320 \mu\text{m}$  and an inner “hole” radius of  $\sim 110 \mu\text{m}$ . The inset of Figure 1 shows the spatial pattern evolution of the pump beam after passing through F2. The pump beam has an expected annular near-field intensity distribution and which could maintain at a distance of  $\sim 14$  mm, covering the entire length of the ceramic. At the position away from the focal plane, the pump beams gradually evolve into a Gaussian-like profile (see the inset of Figure 1). Thus, to spatially match the intensity distribution for the desired LG<sub>01</sub> mode, the ceramic was located at the position where the pump beam with the annular intensity distribution could preserve over the entire length of the ceramic.

The Er:Y<sub>2</sub>O<sub>3</sub> ceramic laser resonator comprised a plane input coupler (IC, anti-reflective coated of  $T > 85\%$  at  $\sim 980$  nm and high reflectivity  $R > 99.8\%$  at 2.65–2.95  $\mu\text{m}$ ) and a plane output coupler (OC) with 10% transmission at the lasing wavelength and a transmission of  $T > 85\%$  at the pump wavelength. A 45° dichroic mirror (DM) was used as a beam splitter to filter the residual pump light in the output beam. Output power and spectrum were recorded using a power meter (Ophir, 3 A-PF-12) and an optical spectrum analyzer of 50-p.m. resolution (AQ6375B, Yokogawa). The pump and output beam profiles were monitored with the aid of an infrared CCD (Xeva-1.7) and a mid-infrared CCD camera (WinCamD-IR-BB), respectively.

## 3 Results and discussion

The Er:Y<sub>2</sub>O<sub>3</sub> ceramic laser output power, as a function of absorbed pump power, is shown in Figure 2. The laser reaches a threshold at an absorbed pump power of  $\sim 1.53$  W and generated 4.65 W of output



power at an absorbed power of 19.8 W, giving a slope efficiency of 25.9% with respect to the absorbed pump power. In comparison with the performance of a previously reported 2.7- $\mu\text{m}$  vortex laser oscillator [23, 24], the output power achieved in the present study was improved by one order of magnitude and the high slope efficiency could be attributed to the mode matching between the annular pump beam and the  $\text{LG}_{0,l}$  mode [26]. We monitored the stability of the output transverse modes and found that it was not maintained with increasing pump power. The inset in Figure 2 shows the output transverse mode profiles at different pump powers. Near the lasing threshold, we observed that output beam profiles were not stable but changed over time. The  $\text{TEM}_{00}$  mode occasionally appeared, but the primary pattern was a petal-like structure with two lobes, which was a result of the coherent superposition of the  $\text{LG}_{0,1}$  modes with opposite helicity [23]. By further increasing the pump power and slightly misaligning the resonator, a clear donut-shaped intensity profile was successfully generated, which is indicative of the single  $\text{LG}_{0,1}$  mode and which was sustained in the pump range from 3.4 to 15.7 W. As the absorbed pump power increased to over 15.7 W, the higher-order  $\text{LG}_{0,2}$  mode was excited.

The underlying mechanism for generation of  $\text{LG}_{0,l}$  modes in an annular pumping scheme can be explained by the mode selection rule. According to the relationship  $P_{\text{th}} \propto A_{\text{eff}}$  [26], the lasing mode that better matches a smaller effective pump ( $A_{\text{eff}}$ ) area exhibits a lower laser threshold and, thus, preferentially oscillates. The effective pump area  $A_{\text{eff}}$  for the  $\text{LG}_{0,l}$  modes can be given by [26]

$$A_{\text{eff}} = \frac{\pi(b^2 - a^2)}{\sum_{i=0}^l \frac{1}{(l-i)!} \left[ \left(\frac{2a^2}{\omega_0^2}\right)^{l-i} \exp\left(-\frac{2a^2}{\omega_0^2}\right) - \left(\frac{2b^2}{\omega_0^2}\right)^{l-i} \exp\left(-\frac{2b^2}{\omega_0^2}\right) \right]} \quad (1)$$

where  $\omega_0$  is the  $\text{TEM}_{00}$  mode waist radius, and  $a$  and  $b$  are the inner and outer radii of the ring-shaped pump beam, respectively. Figure 3 shows the calculated  $A_{\text{eff}}$  values for the  $\text{LG}_{0,l}$  ( $l = 0, 1, \text{ and } 2$ ) modes with respect to the  $\text{TEM}_{00}$  mode waist ( $\omega_0$ ) using the pump size in our

case (an inner radius of 110  $\mu\text{m}$  and an outer radius of 320  $\mu\text{m}$ ). As can be seen, for  $\omega_0 > \sim 290 \mu\text{m}$ , a  $\text{TEM}_{00}$  mode has the lowest  $A_{\text{eff}}$  value and, thus, will be excited preferentially. Decreasing the beam waist to the range of  $205 \mu\text{m} < \omega_0 < 290 \mu\text{m}$ , the  $\text{LG}_{0,1}$  mode will be excited. Furthermore, reducing the beam waist to  $\omega_0 < 205 \mu\text{m}$ , a higher-order  $\text{LG}_{0,2}$  mode can be produced. Therefore, the observed higher modes, i.e.,  $\text{LG}_{0,2}$ , could be explained by that the increased thermal gradient at high pump powers gives rise to serious thermal lens effects, which reduces the sizes of oscillating modes and makes the higher-order mode match well with the pump beam [27].

To confirm this assumption, we measured the thermal focal length ( $f_{\text{th}}$ ) at different ranges of the absorbed pump power. The inset of Figure 3 shows the optical power thermal lens ( $1/f_{\text{th}}$ ) at an absorbed pump power of 7.1 W, 10.7 W, 14.1 W (experimental  $\text{LG}_{0,1}$  mode output), and 18.8 W ( $\text{LG}_{0,2}$  mode output). As can be seen, the thermally induced focal length  $f_{\text{th}}$  decreased with the increase of the pump power, and consequently, the beam size of the  $\text{TEM}_{00}$  mode was calculated and found to be decreased monotonically based on the ABCD matrix, as shown in the inset of Figure 3. To be clear, the calculated mode sizes are depicted in Figure 3 as orange and red dotted lines. As can be seen, the experimentally observed  $\text{LG}_{0,1}$  mode (red dotted line) and  $\text{LG}_{0,2}$  mode (orange dotted lines) fall into the theoretical modeled mode region of the  $\text{LG}_{0,1}$  mode and  $\text{LG}_{0,2}$  mode, respectively. The close agreement between experimental results and the theoretical model is indicative of the  $\text{LG}_{0,l}$  mode excitation and was selected by mode matching, and the topological charge orders were thermally driven.

The normalized transverse intensity distributions of the  $\text{LG}_{0,1}$  mode and  $\text{LG}_{0,2}$  mode output, as a function of the radial position, are shown in Figure 4A. According to the radial intensity distributions for the  $\text{LG}_{0,l}$  mode,  $I_{0,l}(r, \theta, z)$  is obtained as follows [28]

$$I_{0,l}(r, \theta, z) = \frac{2}{\pi(|l|)!} \frac{1}{w(z)^2} \left(\frac{2r^2}{w(z)^2}\right)^{|l|} \exp\left(-\frac{2r^2}{w(z)^2}\right) \quad (2)$$

where  $w(z)$  is the transverse beam radius, and the theoretical intensity distributions of the  $\text{LG}_{0,1}$  mode and  $\text{LG}_{0,2}$  mode are depicted as green and black curves, respectively, in Figure 4A. As can be seen, the measured transverse intensity is in close agreement with the theoretical intensity profiles, which further confirmed the excited laser modes are indeed  $\text{LG}_{0,1}$  and  $\text{LG}_{0,2}$  modes. Typical lasing spectra of the ceramic laser are shown in Figure 4B, and dual wavelength operation at  $\sim 2,717 \text{ nm}$  and  $\sim 2,740 \text{ nm}$  was observed. To select a pure  $\text{LG}_{0,+1}$ ,  $\text{LG}_{0,+2}$ , (or  $\text{LG}_{0,-1}$ ,  $\text{LG}_{0,-2}$ ) mode, an asymmetric cavity loss was introduced by slightly misaligning the OC [29, 30]. The helicity was confirmed by detecting its interference pattern by using the homemade Mach-Zehnder interferometer. As seen in the inset of Figure 4B, the typical fork-shape stripes with one fork indicate that the laser beam oscillated in a pure  $\text{LG}_{0,1}$  mode with  $l = +1$ . We also tried to fine-tune the OC to obtain the  $\text{LG}_{0,-1}$  mode and  $\text{LG}_{0,\pm 2}$  mode, while they were detected but difficult to be maintained over time. Furthermore, the  $\text{LG}_{0,-1}$  and  $\text{LG}_{0,\pm 2}$  mode output with stable well-defined helicity could be achievable by inserting an etalon in the laser resonator to additionally introduce distinguishable loss for the opposite helicity [18, 23].

To further explore the tunability on output beam profiles, we then carefully define the gain distribution in the laser ceramic. This is achieved by adjusting the location of lens F2 against the pump direction to actively control the pump beam intensity distribution

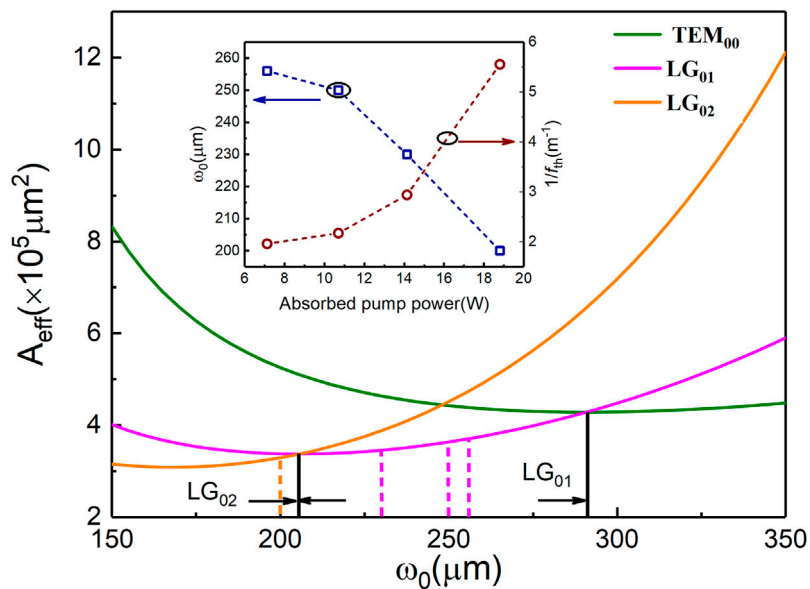


**FIGURE 3** Simulated effective pump area for  $\text{TEM}_{00}$ ,  $\text{LG}_{01}$ , and  $\text{LG}_{02}$  modes. Inset: dependence of the  $\text{TEM}_{00}$  mode radius and the optical power thermal lens on the absorbed pump power.

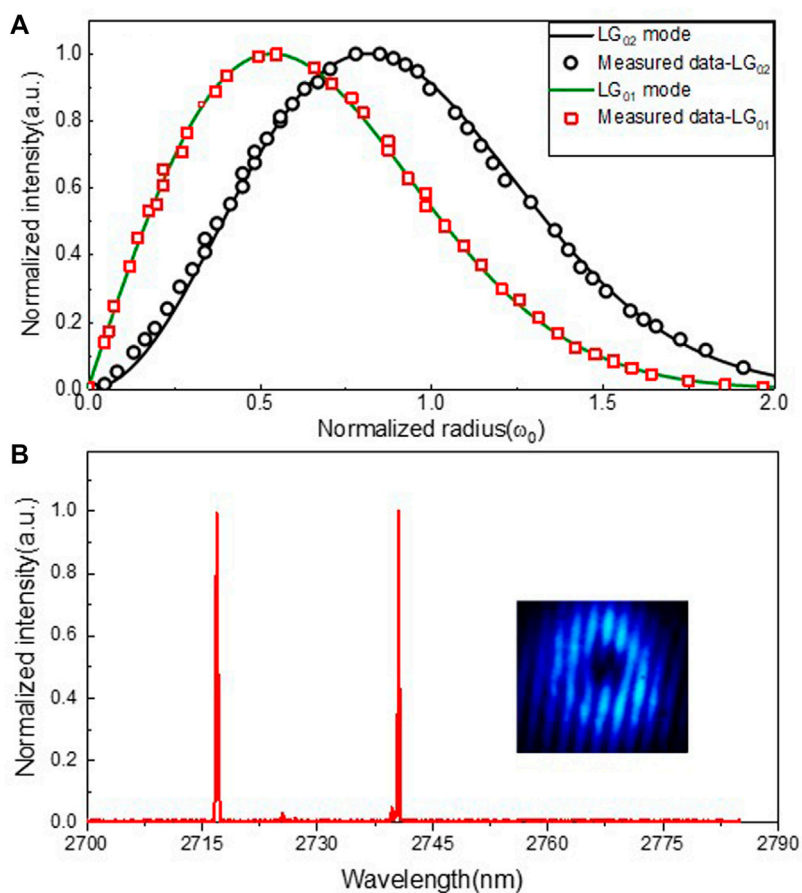


**FIGURE 4** (A) Theoretical and measured transverse intensity distributions for the  $\text{LG}_{01}$  and  $\text{LG}_{02}$  mode (B) output spectra of the vortex laser. Inset: intensity interference pattern of the produced  $\text{LG}_{0,+1}$  mode.

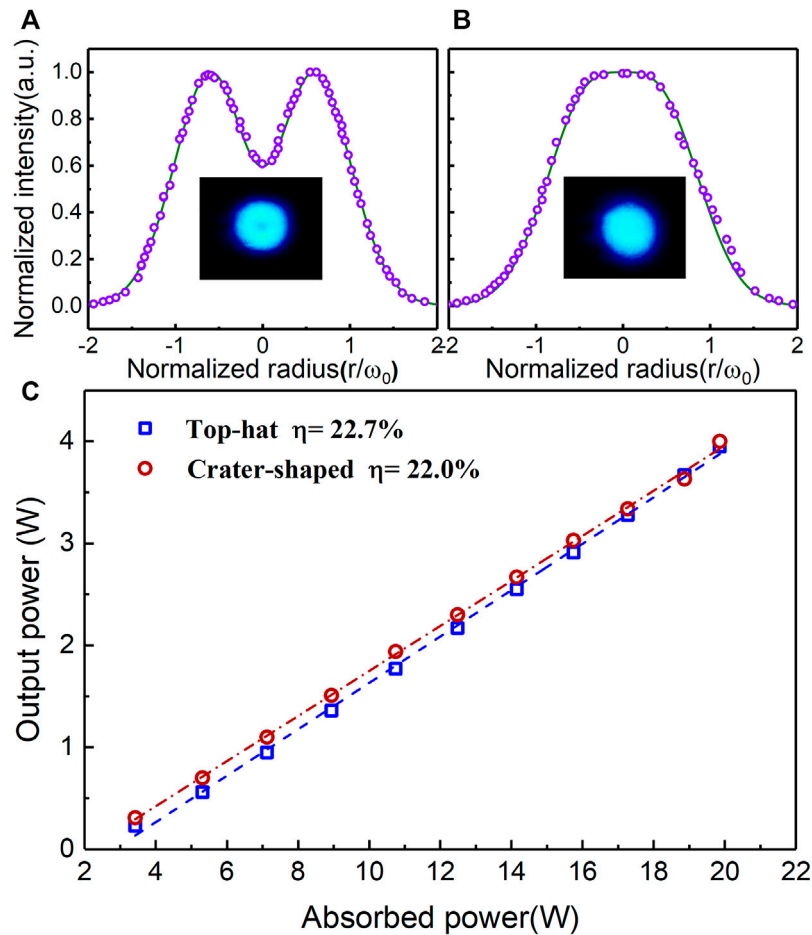


**FIGURE 5**

Beam profiles and measured transverse intensity distributions of the (A) shallow crater-shape mode and (B) quasi-top-hat mode. The solid lines are the normalized theoretical intensity distribution. (C) Laser output power as a function of the absorbed pump power for the shallow crater-shape and quasi-top-hat modes.

in the ceramic, as shown in Figure 1. In other words, benefitting from the pump beam intensity distribution evolution dynamics, the pump region in the ceramic will be fulfilled from annular pump intensity distribution to the existed partial Gaussian-like intensity distribution with gradually translating F2. This combined pump intensity provides available gain in the central volume of the pumped region, which has the highest overlap with  $TEM_{00}$  modes. Therefore, under appropriate pump conditions, the laser will operate in the multimode and the output intensity profile depends on the pump intensity profiles in the ceramic. By continuously translating F2, we observed that the produced beam profiles ranged from the annular intensity pattern, to a shallow crater-shape distribution and, finally, to a quasi-top-hat distribution. Figures 5A, B show the produced shallow crater-shape distribution pattern and quasi-top-hat distribution pattern, respectively. By fitting the normalized transverse intensity distributions with the theoretical model [31], it is indicative that the output profiles are an incoherent superposition of the  $TEM_{00}$  and  $LG_{02}$  modes. The laser output power as a function of absorbed pump power for both beams is shown in Figure 5C. The laser yielded 4 W and 3.9 W of output power for shallow crater-shape beams and quasi-top-hat beams, respectively, at an absorbed pump power of 19.8 W. The corresponding slope efficiency was 22.0% and 22.7%,

respectively, with respect to absorbed pump power. The tailored spatial intensity profiles in the 3- $\mu\text{m}$  spectral region will benefit a range of novel applications, such as scientific research and material processing technology.

## 4 Conclusion

In summary, we have demonstrated the direct generation of high-power  $LG_{0,l}$  beams ( $l = 1, 2$ ) from an  $\text{Er}:\text{Y}_2\text{O}_3$  ceramic laser in the 3- $\mu\text{m}$  spectral region. The pump beams were tailored to possess an annular intensity distribution using a simple capillary fiber to spatially match the desired  $LG_{0,l}$  mode in the laser resonator. Based on the theoretical model for mode selection, we show that the laser was thermally driven and a proper thermal gradient on the ceramic enable the generation of vortex beams with controllable topological charge orders of  $l = 1$  and  $l = 2$ , and no obvious reduction in optical efficiency is observed. The laser generated 4.65 W of output power for an absorbed power of 19.8 W, corresponding to a slope efficiency of 25.9% with respect to the absorbed pump power. Using a simple strategy to define the appropriate gain distribution in the ceramic, spatial intensity distributions ranging from a shallow crater-shape to a distribution

with a quasi-top-hat profile were successfully produced. The laser generated 4 W of output with a shallow crater-shape and 3.9 W of quasi-top-hat intensity profiles, corresponding to a slope efficiency of 22.0% and 22.7%, respectively. Such optical vortices and tailored spatial intensity profiles in the 3- $\mu\text{m}$  spectral region will benefit a range of novel applications, such as super-resolution molecular spectroscopy and fabrication of chiral organic materials.

## Data availability statement

The original contributions presented in the study are included in the article/supplementary material; further inquiries can be directed to the corresponding authors.

## Author contributions

All authors listed have made a substantial, direct, and intellectual contribution to the manuscript and approved it for publication.

## References

- Allen L, Beijersbergen MW, Spreeuw RJC, Woerdman JP. Orbital angular momentum of light and the transformation of Laguerre-Gaussian laser modes. *Phys Rev A* (1992) 45(11):8185–9. doi:10.1103/PhysRevA.45.8185
- He C, Shen YJ, Forbes A. Towards higher-dimensional structured light. *Light Sci Appl* (2022) 11(1):205–17. doi:10.1038/s41377-022-00897-3
- Shen YJ, Wang XJ, Xie ZW, Min C, Fu X, Liu Q, et al. Optical vortices 30 years on: OAM manipulation from topological charge to multiple singularities. *Light Sci Appl* (2019) 8(1):90–29. doi:10.1038/s41377-019-0194-2
- Wang J, Yang JY, Fazal IM, Ahmed N, Yan Y, Huang H, et al. Terabit free-space data transmission employing orbital angular momentum multiplexing. *Nat Photon* (2012) 6(7):488–96. doi:10.1038/NPHOTON.2012.138
- Barreiro JT, Paul TW, Kwiat G. Beating the channel capacity limit for linear photonic superdense coding. *Nat Phys* (2008) 4(4):282–6. doi:10.1038/nphys919
- Heller I, Sitters G, Broekmans OD, Farge G, Menges C, Wende W, et al. STED nanoscopy combined with optical tweezers reveals protein dynamics on densely covered DNA. *Nat Methods* (2013) 10(9):910–6. doi:10.1038/nmeth.2599
- Grier DG. A revolution in optical manipulation. *Nature* (2003) 424(6950):810–6. doi:10.1038/nature01935
- Franke-Arnold S, Allen L, Padgett M. Advances in optical angular momentum. *Laser Photon Rev* (2008) 2(4):299–313. doi:10.1002/lpor.200810007
- Huth F, Govyadinov A, Amarie S, Nuansing W, Keilmann F, Hillenbrand R. Nano-FTIR absorption spectroscopy of molecular fingerprints at 20 nm spatial resolution. *Nano Lett* (2012) 12:3973–8. doi:10.1021/nl301159v
- Tittel FK, Richter D, Fried A. Mid-Infrared laser applications in spectroscopy. In: IT Sorokina KL Vodopyanov, editors. *Solid-state mid-infrared laser sources*. Charm: Springer (2003). p. 458–529. doi:10.1007/3-540-36491-9\_11
- Beijersbergen MW, Coerwinkel RPC, Kristensen M, Woerdman JP. Helical-wavefront laser beams produced with a spiral phaseplate. *Opt Commun* (1994) 112(5-6):321–7. doi:10.1016/0030-4018(94)90638-6
- Marrucci L, Manzo C, Paparo D. Optical spin-to-orbital angular momentum conversion in inhomogeneous anisotropic media. *Phys Rev Lett* (2006) 96(16):163905. doi:10.1103/physrevlett.96.163905
- Bai YH, Lv HR, Fu X, Yang YJ. Vortex beam: Generation and detection of orbital angular momentum [invited]. *Chin Opt Lett* (2022) 20(1):012601. doi:10.3788/COL202220.012601
- Aadhi A, Sharma V, Samanta GK. High-power, continuous-wave, tunable mid-IR, higher-order vortex beam optical parametric oscillator. *Opt Lett* (2018) 43(10):2312–5. doi:10.1364/OL.43.002312
- Furuki K, Horikawa MT, Ogawa A, Miyamoto K, Omatsu T. Tunable mid-infrared (6.3–12  $\mu\text{m}$ ) optical vortex pulse generation. *Opt Express* (2014) 22(21):26351–7. doi:10.1364/OE.22.026351

## Funding

This work is supported by the National Natural Science Foundation of China (62105130, 62035007, and 61875078).

## Conflict of interest

The authors declare that the research was conducted in the absence of any commercial or financial relationships that could be construed as a potential conflict of interest.

## Publisher's note

All claims expressed in this article are solely those of the authors and do not necessarily represent those of their affiliated organizations, or those of the publisher, the editors, and the reviewers. Any product that may be evaluated in this article, or claim that may be made by its manufacturer, is not guaranteed or endorsed by the publisher.

- Camper A, Park H, Lai YH, Kageyama H, Li S, Talbert BK, et al. Tunable mid-infrared source of light carrying orbital angular momentum in the femtosecond regime. *Opt Lett* (2017) 42(19):3769–72. doi:10.1364/OL.42.003769
- Wang YB, Shen YJ, Meng Y, Gong M. Generation of 1535-nm pulsed vortex beam in a diode-pumped Er, Yb: Glass microchip laser. *IEEE Photon Technol Lett* (2018) 30(10):891–4. doi:10.1109/LPT.2018.2822838
- Kim DJ, Kim JW. Direct generation of an optical vortex beam in a single-frequency Nd: YVO<sub>4</sub> laser. *Opt Lett* (2015) 40(3):399–402. doi:10.1364/ol.40.000399
- Lin D, Daniel JMO, Clarkson WA. Controlling the handedness of directly excited Laguerre-Gaussian modes in a solid-state laser. *Opt Lett* (2014) 39(13):3903–6. doi:10.1364/OL.39.003903
- Fang ZQ, Yao Y, Xia KG, Li JL. Actively Q-switched and vortex Nd:YAG laser. *Opt Commun* (2015) 347:59–63. doi:10.1016/j.optcom.2015.02.037
- Ma Y, Vallés A, Tung JC, Chen YF, Miyamoto K, Omatsuet T. Direct generation of red and orange optical vortex beams from an off-axis diode-pumped Pr<sup>3+</sup>: YLF laser. *Opt Express* (2019) 27(13):18190–200. doi:10.1364/OE.27.018190
- Shen YJ, Meng Y, Fu X, Gong M. Wavelength-tunable hermite-Gaussian modes and an orbital-angular-momentum-tunable vortex beam in a dual-off-axis pumped Yb: CALGO laser. *Opt Lett* (2018) 43(2):291–4. doi:10.1364/OL.43.000291
- Ding MM, Chen Y, Wang J, Yin DL, Zhao YG, Shen DY, et al. 2.7  $\mu\text{m}$  optical vortex beam directly generated from an Er:Y<sub>2</sub>O<sub>3</sub> ceramic laser. *Opt Lett* (2019) 44(20):4973–6. doi:10.1364/OL.44.004973
- Gao QG, Zhou JJ, Jia DW, Wang YY, Chen B, Zhao YG, et al. Direct generation of mid-infrared pulsed optical vortices at ~ 2.7  $\mu\text{m}$ . *Opt Express* (2021) 29(25):41842–50. doi:10.1364/OE.444033
- Ding MM, Li XX, Wang F, Shen DY, Wang J, Tang DY, et al. Power scaling of diode-pumped Er: Y<sub>2</sub>O<sub>3</sub> ceramic laser at 2.7  $\mu\text{m}$ . *Appl Phys Express* (2022) 15(6):062004. doi:10.35848/1882-0786/ac6da3
- Kim JW, Clarkson WA. Selective generation of laguerre-Gaussian (LG<sub>0n</sub>) mode output in a diode-laser pumped Nd: YAG laser. *Opt Commun* (2013) 296:109–12. doi:10.1016/j.optcom.2013.01.0461
- Ding YT, Xu MM, Zhao YG, Yu HH, Zhang HJ, Wang ZP, et al. Thermally driven continuous-wave and pulsed optical vortex. *Opt Lett* (2014) 39(8):2366–9. doi:10.1364/OL.39.002366
- Zhang J, Huang SJ, Zhu FQ, Shao W, Chen MS. Dimensional properties of Laguerre-Gaussian vortex beams. *Appl Opt* (2017) 56(12):3556–61. doi:10.1364/AO.56.003556
- Lu JL, Lin FHF, Zhang G, Li BX, Zhang LZ, Chen YF, et al. Direct generation of an optical vortex beam from a diode-pumped Yb:MgWO<sub>4</sub> laser. *Laser Phys Lett* (2017) 14:085807. doi:10.1088/1612-202X/aa7878
- Chen YF, Lan YP. Dynamics of the Laguerre Gaussian TEM<sub>01</sub>\* mode in a solid-state laser. *Phys Rev A* (2001) 63:063807. doi:10.1103/physreva.63.063807
- Kim DJ, Mackenzie JI, Kim JW. Adaptable beam profiles from a dual-cavity Nd:YAG laser. *Opt Lett* (2016) 41(8):1740–3. doi:10.1364/OL.41.001740